第 31卷 第 6期 焊 接 学 报 Vol.31 No.6
2010年 6月 TRANSACTIONS OF THE CHINA WELDING INSTITUTION June 2010

大型框架结构堆焊过程的动态应力及残余应力分析

钟志勇， 傅 卫， 顾轶蓉， 毕 刚
（宝钢设备检修有限公司宝钢机械厂，上海 201900）

钟志勇

摘 要：对大面积激光熔覆和 MIG堆焊过程中结构动态应力演变行为进行了研究. 结果表明，激光熔覆过程在结构中引起的动态应力值较小，远小于结构的屈服强度. MIG焊堆焊过程中动态应力最大值出现在立柱中部位置，最大拉应力为 311.27 MPa，已超过材料的屈服强度；焊后对结构宽度方向的尺寸进行了测量，比原始尺寸增加了 0.4 mm. 用盲孔法测试了堆焊前后结构的残余应力，无论是激光熔覆还是 MIG堆焊，堆焊层局部残余应力均比原始应力有较大的增加，最大应力值均在 220 MPa左右.

关键词：动态应力；残余应力；激光熔覆；堆焊
中图分类号：TG115.28 文献标识码：A 文章编号：0253－360X(2010)06－0093－04

0 序 言

轧机牌坊是热轧机械中的关键设备，长期服役于恶劣的工况条件下其表面会出现了不同程度的腐蚀磨损，使轧机机架与轧辊轴承座间隙难以有效控制管理，影响到板形的控制，对产品质量造成很大影响. 传统机械加工清除牌坊表面受损层找平接触面的修复方法并未改变牌坊表面的性质，使用一段时期后牌坊表面又会受到腐蚀磨损而失效，而且再次（多次）机械加工将会对牌坊的强度和刚度产生不利影响，因此考虑在牌坊窗口面堆焊一层防腐耐磨材料.

对于牌坊类大型结构大面积堆焊修复国内还未见有报道[1]，大面积堆焊过程结构中的应力如何变化，其状态及残余应力会对结构造成什么样的影响，这些均是修复之前想要了解的问题. 多年来学者们对焊接残余应力的测量方法[2]、焊接应力与变形的控制及消除方面做了大量的研究[3,4]，通过对焊接残余应力的测量、控制及消除，改善了构件的使用性能；通过焊接应力与变形的数值模拟[5]，对整个焊接过程中的热力学行为有了更深的认识. 但整个焊接过程结构中的应力应变动态演变的第一手资料还比较缺乏.

文中试验铸造了一个牌坊模拟件，并按实际工况对其进行了大面积堆焊，监测了堆焊过程结构中的应变演变过程，并测试了堆焊后的残余应力，收集了堆焊过程结构中的应变演变的第一手数据，为焊接过程应力应变的演变研究提供一定的方法与思路.

1 试验方法

根据轧机牌坊实物按一定比例缩小，铸造了一个牌坊模拟样，材质为 ZG230－450，加工后其外形尺寸为 1 300 mm×900 mm×201 mm，内框尺寸为 1 000 mm×700 mm×201 mm，在内框侧两垂直面上进行堆焊，试验实物模型如图 1所示.

(a) 激光熔覆焊 (b) 手工气体保护焊

图 1 试验实物模型
Fig.1 Testing model

堆焊过程分两次进行，第一次先使用激光熔覆的方法利用机械手自动堆焊，焊层厚度约为 0.5 mm. 从内框底部向顶部顺序焊接，堆焊完一侧后再堆焊另一侧. 第二次堆焊时先铣削加工去除激光熔

收稿日期：2009－02－12

覆层及其影响区域，去除厚度约为 2 mm，然后用 MIG焊堆焊两层不锈钢材料. 第一层堆焊顺序同激光熔覆的顺序，第二层左右交替堆焊.

采用 16通道应变测试仪对堆焊过程中结构动态应力进行测量，TMI焊接式高温应变计粘贴于牌坊模拟样左侧立柱，监测了 6个特征点水平和垂直方向的应力变化过程，具体贴片位置如图 2所示. 用手提电脑内专用的软件记录实时的应变演化数据，数据采集频率为 20 Hz. 采用的高温应变计具有温度自补偿功能，可以有效减少温度对测量数据的影响. 由于高温对应变计的灵敏度、热输出都有很大的影响，为了保证测量数据的准确性，采取相应的措施对采集的数据进行了修正. 堆焊过程中用红外测量仪对结构的温度进行了测量记录.

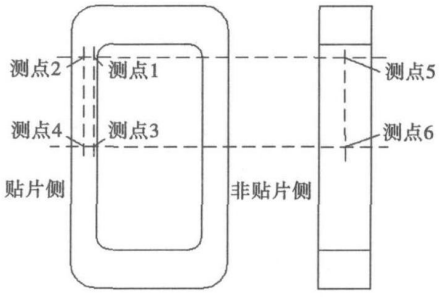

图 2 动态应力测试点的位置

Fig. 2 Position of each testing point

残余应力的测量采用盲孔法，测量被测表面的平面应力. 应变片采用上海应变计厂生产的盲孔法专用 CA-120型 0°~90°~45°三向应变花，应变测量仪为上海华东电子仪器厂生产的 YJ-16静态电阻应变仪. 在获得盲孔法实测应变后，再用盲孔法专用计算公式求得测点残余应力. 残余应力测量点位于堆焊表面及其侧面，具体位置取右侧立柱并与动态应力测量点位置相对应.

2 试验结果及讨论

2.1 堆焊过程中的动态应力分析

2.1.1 激光熔覆过程中的应力应变演变

对激光熔覆过程中各测点的应变演变进行了监测，通过转换成相应的应力值进行分析比较。从非贴片侧激光熔敷过程中的应变演变结果发现，测点 3水平方向产生了一压应变且缓慢上升，应变最大为 -1.02×10^{-4}，相当于 −21 MPa；垂直方向同样也产生了压应变，应变值上升到一较小幅值后基本不再变化，应变最大值为 -1.59×10^{-4}，相当于 −33.1 MPa. 采用红外温度测量仪对焊枪周边区域进行测量，金属表面温度不到 100 ℃，表明非贴片侧激光熔覆时金属受热膨胀对贴片侧虽产生了一定的挤压作用，但由于激光熔敷时热输入相对较小，框架结构一侧激光熔敷时对另一侧的应变变化影响不大.

在贴片侧从立柱的下部向上部堆焊过程中，当堆焊进行到测点 3位置即立柱的中间部位时，测点 3和测点 4的垂直应变出现一个峰值，对应一个拉应力峰值. 当堆焊越过测点 3时，其垂直应力又趋向于压应力. 同样当堆焊进行到测点 1时，靠近焊接区域的测点 1垂直方向出现一个拉应力峰值，但当堆焊越过测点 1时，测点 1和测点 2的垂直应力又趋于压应力。测点 3的应力峰值要大于测点 1的应力峰值，各点对应的应变演变如图 3所示.

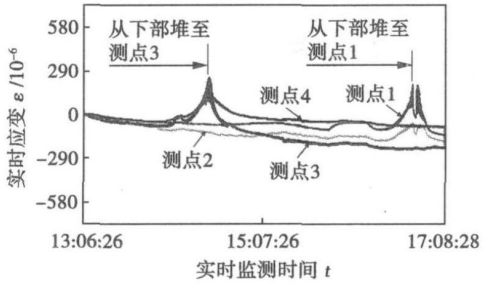

图 3 激光熔覆过程中贴片侧测点垂直方向的应变演变

Fig. 3 Strain evolution in vertical direction of each testing point during laser cladding process

在堆焊的初始阶段，测点 1、测点 2和测点 3的水平应变皆为压应变. 当激光熔覆进行至测点 3时，其水平应变迅速增大变为拉应变，熔敷过程离开测点 3时，其水平拉应变基本保持不变. 同样当熔敷过程进行到测点 1时，其水平方向的应变由压应变转变为拉应变，越过该点时应变值保持不变. 而测点 2的水平应变在激光熔覆由下往上的过程中，压应变一开始逐渐变大，在越过该点时应变值有所减小，如图 4所示.

贴片侧激光熔覆过程中，测点 1的最大拉应力为 21.03 MPa，方向与水平方向成 1.73°的夹角；最大压应力为 −30.38 MPa，与垂直方向成 9.85°的夹角. 测点 3的最大水平拉应力为 32.67 MPa，最大垂直压应力为 −50.3 MPa. 立柱背面测点 5和测点 6的应变变化较小，测点 6的最大压应力为 −13.32 MPa.

2.1.2 电弧堆焊过程中的应力应变演变

电弧堆焊焊接了两层，在对非贴片侧进行第一层堆焊时测点 3的垂直应变最大为 -2.03×10^{-4}，

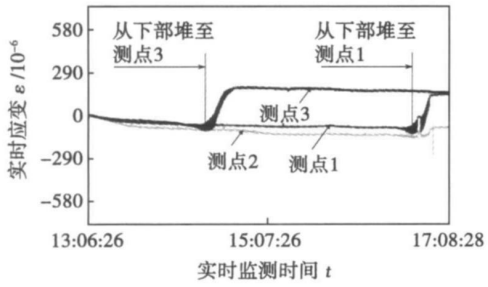

图 4　激光熔覆过程中贴片侧各测试点水平方向的应变演变

Fig. 4　Strain evolution in horizon direction of each testing point during laser cladding process

相当于 −42 MPa；水平应变最大为 8.27×10⁻⁴，相当于 171 MPa；在对贴片侧进行第一层堆焊时，测点 1的最大拉应力为 143.4 MPa，与水平方向成 1.86°的夹角；最大压应力为 −32.84 MPa。测点 3的垂直应变最大为 8.95×10⁻⁴，相当于 185.2 MPa；水平应变最大为 8.39×10⁻⁴，相当于 173.8 MPa。测点 6的垂直最大拉应力为 36.34 MPa，最大压应力为 −9.2 MPa。

第二层的堆焊过程中，贴片侧和非贴片侧的堆焊交替进行，当贴片侧的第二层堆焊进行到测点 3和 4时，其垂直方向出现了一个拉应变峰值，离焊接区域较远的测点 4应变峰值和变化的幅值均小于测点 3. 同样当第二层堆焊进行到测点 1位置时，测点 1和测点 2的垂直应变也出现一个拉应变峰值，且测点 2的峰值和变化幅值均小于测点 1. 总体上在垂直方向测点 3的垂直应变峰值最大，测点 1次之，$\varepsilon_{V3} > \varepsilon_{V1} > \varepsilon_{V4} > \varepsilon_{V2}$，如图 5所示.

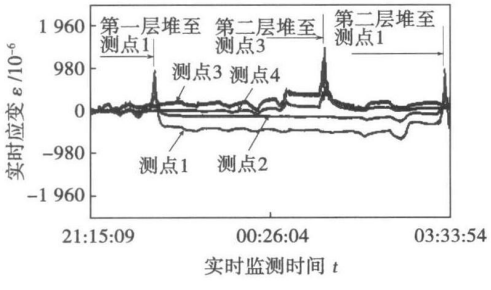

图 5　MIG堆焊过程贴片侧测点垂直方向的应变演变

Fig. 5　Strain evolution in vertical direction of each testing point during MIG overlaying welding process

当第二层堆焊进行到测点 3位置时，其水平拉应变再一次增大，当堆焊离开此位置时，其拉应变保持在这一水平. 同样当第二层堆焊进行到测点 1位置时，测点 1和测点 2的水平拉应变也再一次增大，并保持在一个稳定的水平. 总体比较，在水平方向测点 3的水平应变幅值最大，测点 1次之，$\varepsilon_{H3} > \varepsilon_{H1} > \varepsilon_{H2}$，如图 6所示.

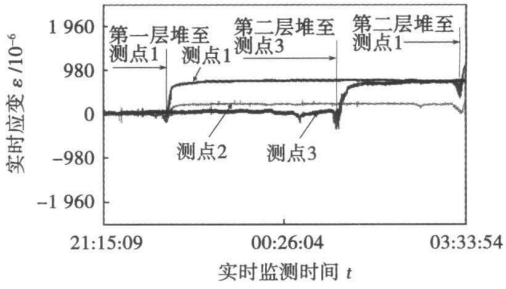

图 6　MIG堆焊过程中贴片侧测点水平方向的应变演变

Fig. 6　Strain evolution in horizon direction of each testing point during MIG overlaying welding process

在整个第二层的堆焊过程中，测点 1的最大拉应力为 219.2 MPa，方向与水平方向成 1.9°的夹角，最大压应力为 −83.05 MPa。测点 3的水平最大拉应力为 311.27 MPa。在立柱背面测点 5和测点 6的应变变化同样都不大，测点 6对应的过程最大拉应力为 26.89 MPa，最大压应力为 −14.2 MPa。

2.1.3　动态应力结果讨论

由前文数据可以得知，激光熔覆和 MIG堆焊方法相比，激光熔覆过程中各测试点的应力峰值远小于材料屈服强度和 MIG堆焊过程中的应力峰值. 低的热输入以及薄的熔敷层使得激光熔覆过程对这种大型框架结构内的应力应变变化影响不大. MIG堆焊过程中测点 3即立柱的中间部位出现了应力峰值，最大拉应力为 311.27 MPa，已超过基体材料的屈服强度. 在立柱的上部接近窗口直角处的测点 1最大拉应力为 219.2 MPa，也接近于基体材料的屈服强度. 这均说明在 MIG堆焊过程中框架结构材料局部发生了屈服，产生了塑性变形. 堆焊后对该结构宏观尺寸进行了测量. 结果表明，激光熔覆后结构没有发生变形，而 MIG堆焊后框架宽度上变大了 0.4 mm，即 MIG堆焊后结构发生了宏观变形. 这与各测点峰值应力均为拉应力，并有部分峰值应力超过材料屈服强度的监测结果是吻合的.

从监测过程也可以发现，从立柱的下部往上部顺序堆焊过程中，焊至测点位置时该点垂直方向的应力会迅速增大至一相对峰值，焊接越过该点的冷却过程中又逐步回复至初始值附近，而水平方向的应力每焊至该点时应力水平上升一个台阶并在随后的冷却过程中保持不变，随着堆焊层数和厚度的增加，

应力累加直至超过材料的屈服极限产生塑性变形.

2.2 残余应力测试结果分析

分别测量了模拟件的原始残余应力状态,激光熔覆后以及 MIG堆焊后结构中各测试点的残余应力.三种状态下的最大主应力计算结果如表 1所示.

表 1 三种状态下各测点的残余应力

Table 1 Residual stress of each testing point in different status

测点号	原始状态残余应力 σ_1/MPa	激光熔覆后残余应力 σ_2/MPa	MIG堆焊后残余应力 σ_3/MPa
测点 1	49	84	131
测点 2	72	43	163
测点 3	52	89	287
测点 4	65	139	109
测点 5	66	227	206
测点 6	89	220	245

根据表 1所测残余应力值可知牌坊模拟件原始状况应力水平不高,最大主应力在 90 MPa以下.

从激光熔覆后的残余应力结果可以看出,框架侧面应力有所上升,但幅度不大.测点 1和测点 3约达 90 MPa,但测点 2略有下降,为 43 MPa,测点 4上升较大达 139 MPa.测点 5和测点 6为同一个测点,为激光熔覆层表面,钻孔钻了两次,第一次钻孔深度约为 1 mm,第二次钻到基体,两次计算的应力值比较接近,说明应变已经释放完,最大主应力达 220 MPa,也说明激光熔覆使表面残余应力上升,涂层表面残余应力已接近基体材料屈服强度.

从不锈钢堆焊层的残余应力结果可以看出,残余应力水平明显上升,其中侧面中央贴近堆焊面的测点 3达 287 MPa,已达到基体材料屈服应力.主要是由于多次堆焊和机加工的热应变强化和加工硬化响应而造成.堆焊面应力约为 220 MPa,略低于测点 3的水平,主要是由于不锈钢的低温相变,使母材残余应力达到峰值后堆焊面再出现下降而造成.

3 结 论

(1)激光熔覆过程中各测试点的应力峰值远小于材料屈服强度和 MIG堆焊过程中的应力峰值.而 MIG大面积堆焊过程中产生的应力峰值已超过材料的屈服强度,引起了结构的宏观变形.

(2)激光熔覆和 MIG堆焊后的涂层表面残余应力均已接近或超过基体的屈服强度.

(3)试验提供了大型框架结构大面积堆焊过程结构应变演变的第一手资料,为焊接过程的应力应变的演变研究提供一定的方法与思路.

参考文献:

[1] 罗喜泽. 层叠堆焊法在大型零件修复上的应用[J]. 钢管, 2004, 33(4): 47-50.
Luo Xize. Application of overlaying welding process to repair of large-sized component[J]. Steel Pipe, 2004, 33(4): 47-50.

[2] 陈会丽, 钟 毅, 王华昆, 等. 残余应力测试方法的研究进展[J]. 云南冶金, 2005, 34(3): 52-55.
Chen Huili, Zhong Yi, Wang Huakun, et al. Research progress of the method for residual stress measurement[J]. Yunnan Metallurgy, 2005, 34(3): 52-55.

[3] 李 军, 杨建国, 翁路露, 等. 薄壁结构焊接的焊中控制研究现状[J]. 焊接, 2008(8): 16-22.
Li Jun, Yang Jianguo, Weng Lulu, et al. Research status of the welding in-process control of thin-walled structures[J]. Welding & Joining, 2008(8): 16-22.

[4] 宗 培, 曾宏军. 焊接过程对焊接残余应力及残余变形的影响[J]. 海军工程大学学报, 2002, 14(4): 77-80.
Zong Pei, Zeng Hongjun. Effect of welding procedure on welding residual stress and strain[J]. Journal of Naval University of Engineering, 2002, 14(4): 77-80.

[5] 张建强, 赵海燕, 吴 甦, 等. 焊接过程三维应力变形数值模拟研究进展[J]. 焊接学报, 2003, 24(5): 91-96.
Zhang Jianqiang, Zhao Haiyan, Wu Su, et al. Research progress of numerical simulation of three-dimensional welding stress and distortion in welding process[J]. Transactions of the China Welding Institution, 2003, 24(5): 91-96.

作者简介:钟志勇,男,1970年出生,硕士,工程师.主要从事冶金设备的表面修复工作.发表论文 1篇.

Email: zhongzhiyong@baosteel.com

structure; low temperature impact resistance

Property analysis and brazing preparation of NiTi/NiTiNb composite sheet ZHAO Xingke, TANG Jiawei, HUANG Jihua, ZHANG Hua (School of Materials Science and Engineering, Beijing Science and Technology University, Beijing 100083, China). p. 73—76, 80

Abstract: The microstructure of interface and bending deformation behavior of composite sheet, which was brazed by AgCu eutectic brazing alloy, were investigated. The results reveal that the brazing joint has good mechanical properties, and the bending angle of the brazed plates reaches 120° at room temperature or 0 ℃ without fracture. The composite sheet shows good shape memory effect, and the shape recovery temperature has a larger range between the shape recovery temperatures of these two alloys, which is resulted by the deformation compatibility of the two alloys. The stress-strain curves of the composite sheet show obvious hysteretic loop and indicate good damping characteristic at room temperature or 0 ℃.

Key words: brazing; shape memory alloy; composite sheet; stress-strain

Microstructure and solderability of Sn-9Zn-xCe lead-free solder HU Yuhua, XUE Songbai, CHEN Wenxue, WANG Hui (College of Materials Science and Technology, Nanjing University of Aeronautics and Astronautics, Nanjing 210016, China). p. 77—80

Abstract: Effects of rare earth element Ce added in Sn-9Zn solder on the microstructure and spreading property as well as mechanical properties were investigated. Results indicate that with the increase of the Ce from 0 to 0.08%, the microstructure is refined obviously and Zn-rich phrase is decreased. While the content of Ce exceeds 0.08%, small block Sn-Ce intermetallic compounds will appear. Results also show that with the increase of the Ce, the spreading property is improved, the spreading area reaches maximum when the content of Ce is up to 0.08%, and the best mechanical properties of the soldered joints are achieved while the content of Ce is about 0.08%.

Key words: rare earth element Ce; lead-free solder Sn-Zn; spreadability; mechanical properties; microstructure

Design of supersonic flame spraying gun with combustion-supporting of air-oxygen and liquid fuel JIA Peng, WANG Zhiping, LIN Ya, LI Yajuan (College of Science, Civil Aviation University of China, Tianjin 300300, China). p. 81—84

Abstract: A supersonic flame spraying gun in which liquid fuel and air-oxygen are mixed in chamber to improve combustion stability by flameholder was obtained. The speed and temperature of jet from the gun was measured by the Spraywatch monitor system. The microstructure and properties of the WC-12Co coatings produced by the gun were investigated. The results indicate that the jet speed exceeds 1 300 m/s, and the adjustable range of temperature is 2 302 K to 3 410 K, which an accuracy of adjustment reaches ±50 K. The WC retention rate in the coating increases with the increasing of air and oxygen mixing ratio, and so the hardness of coatings increases. The thickness of the coating obtained by spraying with air-supporting combustion is over 5 mm.

Key words: supersonic flame spraying gun; flameholder; air-oxygen combustion-supporting; WC-12Co coating

Effects of aging on shearing strength and fracture surface characteristics of SnCuSb/Cu soldering joint MENG Gongge[1], LI Dan[1], LI Zhengping[1], WANG Yanpeng[1], CHEN Leida[2] (1. School of Material Science & Engineering, Harbin University of Science and Technology, Harbin 150040, China; 2. School of Material Science & Engineering, Dalian University of Technology, Dalian 116024, Liaoning, China). p. 85—88

Abstract: The effects of 150 ℃ aging on the shearing strength and fracture surface characteristics of Sn-0.7Cu-xSb/Cu (x=0, 0.25, 0.5, 0.75, 1.0) soldering joints were studied by scanning electron microscopy and energy dispersive X-ray spectrometry. The results indicate that the shearing strength of the joint increases with the increasing of Sb in solder and reduces remarkably with the increasing of aging time. The location of fracture is at the solder and appears at interface between the solder and the intermetallic compound of Cu_6Sn_5. Fracture for post soldering specimen with a lot of dimples on its surfaces occurs mainly at the solder and the fracture type is ductile. With the increasing of aging time, the fracture location trends to half solder and half interfacial intermetallic compound. In 500 h aging, Cu_3Sn can be seen at fracture surface which transfers to brittleness from ductileness.

Key words: soldering joints; shearing strength; aging; fracture surface; SnCuSb

Microstructure and corrosion resistance of butt joint of 1Cr18Ni9Ti+Q235 composite plate WANG Wenxian[1], WANG Yifeng[1], LIU Mancai[1], CHENG Fuchang[1], WU Wei[2] (1. College of Materials Science and Engineering, Taiyuan University of Technology, Taiyuan 030024, China; 2. Taiyuan Yangguanyuan Stainless Steel Co., Ltd., Taiyuan 030008, China). p. 89—92

Abstract: Four different automatic welding techniques were applied for butt welding of the composite pipe that has a clad layer of 1Cr18Ni9Ti with a thickness of 3 mm and a substrate layer of Q235 with a thickness of 10 mm. The properties of the joint, including microstructure, tensile strength, bend strength, impact toughness, electrochemical and intergranular corrosion resistance, were evaluated. The results indicate that the phase of the clad layer welded by tungsten inert gas welding (TIG) is austenite with a little ferrite. The electrochemical corrosion resistance of the joint is similar to that of the base metal in hydrochloric acid of 1 mol/L and no intergranular corrosion is observed. The phase of the TIG welded joint of the substrate layer is martensite laths that have high strength and excellent toughness. But both the joints of the substrate layer and the clad layer welded by submerged arc welding have poorer mechanical properties and corrosion resistance, respectively.

Key words: stainless steel; composite plate; welding technique; mechanical properties; corrosion resistance

Analysis of dynamic and residual stresses in overlaying process of large frame construction ZHONG Zhiyong, FU Wei, GU Yirong, BI Gang (Baosteel Equipment Maintenance Co., Ltd., Baosteel Machinery Factory, Shanghai 201900, Chi-

Abstract: The structural dynamic stresses in the process of large area overlaying by using laser cladding and MIG welding methods were observed. The results show that the maximum dynamic stress is much lower than the yield stress of the structure in the process of laser overlaying but greater than the yield stress in the process of MIG overlaying welding, and the maximum tensile stress which produced in the middle of the structure is 311.27 MPa. The dimension increases 0.4 mm in width after the MIG overlaying welding. The maximum residual stresses measured by hole-drilling method after the laser overlaying welding or MIG overlaying welding reaches about 220 MPa both.

Key words: dynamic stress; residual stress; laser cladding; overlaying

Abstract: Based on thermal elastic-plastic theory, X80 pipeline steel welding temperature fields and stress fields were simulated with SYSWELD and double ellipsoid thermal source model. Residual stress distributions were obtained. The residual stresses are rather large in the welded seam zones and the adjacent zones and gradually reduce away in the base metal. The cooling velocity difference between the surface and the inner of the pipeline results in opposite directions or different levels of residual stresses. Effects of weld parameters on residual stresses are investigated, and the results show that the residual stress decreases with the increase of heat inputs or preheats. High heat inputs and preheats should be applied to reduce welding residual stresses.

Key words: pipeline steel; numerical simulation; welding residual stresses; double ellipsoid thermal source

Abstract: The nano-scale marble electrode was made, which conventional micron-scale marble in the coating of D600R, a hardfacing shielded metal-arc welding electrode, was replaced by nano-scale marble ($CaCO_3$) with particles size ranges of 70—90 nm. The welding current, arc voltage and short-circuiting time were measured with an arc characteristics analyzer (Hannover analystor), and the arc characteristics of the micron-scale marble and nano-scale marble electrodes were obtained. By means of welding procedure test, hydrogen test, melting temperature and hardness measuring, wear test and micro-analysis, the welding processing properties and mechanical properties of deposited metal of the two electrodes were studied respectively. The results show that when micron-scale marble is replaced by nano-scale marble, the melting temperature of coating and the amount of diffusible hydrogen in deposited metal are decreased, and the deposition efficiency of electrode is increased, the probability density sum of short-circuiting voltage and short-circuiting current, and the sum of short-circuiting time, including over 2.05 m/s, are all decreased, and the electrode operating properties are improved, the hardness and wear resistance of deposit metal are enhanced.

Key words: nano-scale marble; surfacing electrode; electrode properties

Abstract: A numerical simulation system of welding was developed for studying welding thermal process, welding stress/strain and welding deformations. A mesh-oriented data modeling method was applied to solve the problem which is too difficult to use normal FEM software to simulate welding thermal process, stress/strain and deformation of typical aircraft components. The simulation system was designed by using object-oriented method. Operating the system, a customer could simply input the geometry parameters, such as mesh size, welding thermal source parameters, fixing position and welding sequence, into the user interface. All the data input were changed into auto simulation information through the calculation of the system core class. After that, the auto simulation information was converted into Marc command stream which would be loaded by the wheeling Marc process on the background, and calculating the result data of welding thermal process, stress/strain and deformation can predict and analyze the welding stress and deformation.

Key words: aircraft components; auto welding simulation; temperature field; stress/strain field; Marc software

Abstract: The 6063 Al alloy joint using Cu cladding as reaction layer was obtained by contact-reaction brazing method. The typical interfacial structure of the joint was analyzed, and also the effect of microelement on interface structure and joint strength were emphasized. The results show that the brazing interface consists of Al_2Cu, α-Al, Mg_2Si and ω-$Fe_1Cu_2Al_7$, the existence of Fe results in formation of ω-$Fe_1Cu_2Al_7$ lath-shaped phase and weakens the joint shearing strength, and Mg and Si elements enriches in the center of brazing seam as Mg_2Si phase and exacerbates with the extension of holding time. The shearing strength of the joint is mainly controlled by the category and feature of interfacial products and the extent of isothermal solidification, and the highest average shearing strength of the joint can reach 105.3 MPa at brazing temperature of 570 ℃ and holding for 60 min.

Key words: 6030 aluminum alloy; contact reaction brazing; interfacial structure; shearing strength